

International Journal of Modern Physics E
© World Scientific Publishing Company

UTILIZING HIGH- p_{\perp} THEORY AND DATA TO CONSTRAIN THE INITIAL STAGES OF QUARK-GLUON PLASMA

BOJANA ILIC

*Institute of Physics Belgrade, University of Belgrade, Pregrevica 118
Belgrade, 11080, Serbia
bojanab@ipb.ac.rs*

DUSAN ZIGIC

*Institute of Physics Belgrade, University of Belgrade, Pregrevica 118
Belgrade, 11080, Serbia
zigic@ipb.ac.rs*

MARKO DJORDJEVIC

*Faculty of Biology, University of Belgrade, Studentski trg 16
Belgrade, 11000, Serbia
dmarko@bio.bg.ac.rs*

MAGDALENA DJORDJEVIC

*Institute of Physics Belgrade, University of Belgrade, Pregrevica 118
Belgrade, 11080, Serbia
magda@ipb.ac.rs*

Received Day Month Year

Revised Day Month Year

The scarce knowledge of the initial stages of quark-gluon plasma before the thermalization is mostly inferred through the low- p_{\perp} sector. We propose a complementary approach in this report - the use of high- p_{\perp} probes' energy loss. We study the effects of four commonly assumed initial stages, whose temperature profiles differ only before the thermalization, on high- p_{\perp} R_{AA} and v_2 predictions. The predictions are based on our Dynamical Radiative and Elastic ENergy-loss Approach (DREENA) framework. We report insensitivity of v_2 to the initial stages, making it unable to distinguish between different cases. R_{AA} displays sensitivity to the presumed initial stages, but current experimental precision does not allow resolution between these cases. We further revise the commonly accepted procedure of fitting the energy loss parameters, for each individual initial stage, to the measured R_{AA} . We show that the sensitivity of v_2 to various initial stages obtained through such procedure is mostly a consequence of fitting procedure, which may obscure the physical interpretations. Overall, the simultaneous study of high- p_{\perp} observables, with unchanged energy loss parametrization and restrained temperature profiles, is crucial for future constraints on initial stages.

Keywords: quark-gluon plasma; initial stages; jet quenching.

PACS numbers: 12.38.Mh; 24.85.+p; 25.75.-q

1. Introduction

In ultrarelativistic heavy-ion collisions (HIC) at the Relativistic Heavy Ion Collider (RHIC) and the Large Hadron Collider (LHC) (commonly termed as mini big bangs), a new form of matter — the quark-gluon plasma (QGP),^{1,2} in which quarks, antiquarks, and gluons are deconfined, is created. The large transverse momentum (high- p_{\perp}) particles are formed immediately upon the collision and therefore are affected by all stages of QGP evolution. This makes them excellent probes^{3,4} of this new state of matter, primarily through two main energy loss-based high- p_{\perp} observables — angular averaged (R_{AA}) and angular differential (v_2) nuclear modification factors.

Traditionally, rare high- p_{\perp} probes ($p_{\perp} \gtrsim 5$ GeV), which present $\sim 0.1\%$ of all particles produced in HIC, are used for studying the mechanisms of jet-medium interactions, while low- p_{\perp} sector^{5–7} ($p_{\perp} \lesssim 5$ GeV) is used to infer QGP features, such as e.g. initial stages before the QGP thermalization. However, up-to-date initial-stage properties are poorly known. Therefore, the need for an alternative approach to assessing the initial-stage features emerged. We here propose using high- p_{\perp} probes as a complementary tool for this purpose, primarily since high- p_{\perp} partons are good probes of QGP properties, where these properties depend on initial QGP stages. Furthermore, the recently acquired extensive set of high-precision experimental data for the two aforementioned high- p_{\perp} observables^{8–13} facilitates our study. This issue is moreover intriguing, as results of current theoretical studies on this subject are mostly inconclusive.^{14–16}

A more rigorous study on this issue is required, that implies higher control over both the energy loss model and the analyzed temperature profiles. To accomplish this, we apply a full-fledged DREENA-B¹⁷ framework (B stands for one-dimensional (1D) Bjorken¹⁸ expansion), based on our state-of-the-art dynamical energy loss formalism¹⁹ that will be outlined in the next section. It also considers 1D Bjorken¹⁸ medium evolution, which is highly suitable for this study, as it allows the analytical introduction of different evolutions before thermalization, with the same evolution after thermalization, which facilitates the isolation of the effects of different initial stages. Additionally, we checked that the transition from 1D Bjorken to full 3+1D hydrodynamical evolution²⁰ does not significantly change our high- p_{\perp} predictions, implying that for reliable high- p_{\perp} predictions, an accurate energy loss model is more important than the medium evolution model. Therefore, DREENA-B¹⁷ provides an optimal framework for the initial-stages study, as it combines a state-of-the-art energy loss model with fully controlled temperature profiles. Note that, in this paper, we provide a part of the more detailed results obtained in Ref. 21, enriched with some complementary predictions.

2. Numerical and Theoretical Framework

For generating medium modified distribution of high- p_\perp particles, irrespective of their flavor, we apply the generic pQCD convolution formula:^{19,22}

$$\frac{E_f d^3\sigma}{dp_f^3} = \frac{E_i d^3\sigma(Q)}{dp_i^3} \otimes P(E_i \rightarrow E_f) \otimes D(Q \rightarrow H_Q), \quad (1)$$

where i and f stand for the initial parton (Q) and final hadron (H_Q), respectively. The initial parton momentum distribution $\frac{E_i d^3\sigma(Q)}{dp_i^3}$ is calculated in accordance with Ref. 23. The energy loss probability $P(E_i \rightarrow E_f)$ is based on our dynamical energy loss formalism (see paragraph below) and incorporates multigluon²⁴ and path-length fluctuations.^{22, 25, 26} $D(Q \rightarrow H_Q)$ denotes fragmentation function, where for the light hadrons, D and B mesons de Florian-Sassot-Stratmann (DSS),²⁷ Braaten-Cheung-Fleming-Yuan (BCFY)²⁸ and Kartvelishvili-Likhoded-Petrov (KLP)²⁹ fragmentation functions are used, respectively.

As a crucial ingredient of the calculations, we employ our state-of-the-art dynamical energy loss formalism,^{30–32} which includes: 1) Dynamical QCD medium of a finite temperature and a finite size, so that the energy exchange with the medium constituents is taken into account as opposed to static scattering centers case. It also considers that the medium created in ultrarelativistic heavy-ion collisions has a finite size, and that initial partons are created inside the medium. 2) The calculations are based on the finite temperature field theory and generalized hard-thermal-loop approach,³³ generically regulating infrared divergences. 3) Both collisional³² and radiative^{30, 31} energy loss mechanisms are included and performed within the same theoretical framework, so that no interference or overlapping occurs between them. 4) The formalism is generalized to the case of finite magnetic mass³⁴ and running coupling.¹⁹ Chromomagnetic (μ_M) to chromoelectric mass (μ_E) ratio is estimated to be in a range $0.4 - 0.6$ by different non-perturbative approaches.^{35, 36} Hence, in this paper we assume $\mu_M/\mu_E = 0.5$. Our most recent advancement within formalism is the relaxation of the widely used soft-gluon approximation.³⁷ In Ref. 38, we demonstrated that all the above ingredients are necessary to accurately reproduce high- p_\perp suppression data.

The full-fledged analytical expressions for single gluon radiation spectrum and collisional energy loss per unit length in an expanding medium are given by Eqs. (6) and (2) from Ref. 17, respectively. Thereby, the standard values for heavy and light quark masses are considered ($M_c = 1.2$ GeV, $M_b = 4.75$ GeV, while for light quarks thermal masses are assumed).

Further, we assume that the medium expansion model is given by the ideal hydrodynamical 1D Bjorken expansion,¹⁸ *i.e.*, $T(\tau) \sim \sqrt[3]{(\tau_0/\tau)}$ (where τ is a proper time), with thermalization time set at $\tau_0 = 0.6$ fm/c.³⁹ The detailed determination of initial QGP temperature T_0 for the considered centrality range is provided in Ref. 17. For brevity, here we focus on 30 – 40% centrality region in $\sqrt{s_{NN}} = 5.02$ TeV $Pb+Pb$ collisions at the LHC, which corresponds to $T_0 = 391$ MeV,¹⁷ although

4 *Bojana Ilic, Dusan Zigic, Marko Djordjevic, Magdalena Djordjevic*

we checked that the same conclusions apply regardless of the considered centrality bin. The QGP transition temperature is assumed to be $T_C \approx 160$.⁴⁰

Finally, we provide the expressions for two main high- p_\perp observables. The angular averaged nuclear modification factor R_{AA} is defined as the ratio of the quenched p_\perp -spectrum in $A + A$ collisions with respect to $p + p$ collisions, normalized by the number of binary collisions N_{bin} :

$$R_{AA}(p_T) = \frac{dN_{AA}/dp_T}{N_{bin}dN_{pp}/dp_T}. \quad (2)$$

However, an alternative form²⁶

$$R_{AA} \approx \frac{R_{AA}^{in} + R_{AA}^{out}}{2}, \quad (3)$$

is also used for providing more intuitive insight in the underlying mechanisms. Here¹⁴ $R_{AA}^{in} = \frac{dN_{AA}/dp_T d\phi|_{\phi=0}}{N_{bin}dN_{pp}/dp_T d\phi|_{\phi=0}}$ ($R_{AA}^{out} = \frac{dN_{AA}/dp_T d\phi|_{\phi=\pi/2}}{N_{bin}dN_{pp}/dp_T d\phi|_{\phi=\pi/2}}$) stands for in-(out-of-)plane nuclear modification factor. The high- p_\perp elliptic flow is given by the expression:^{26, 41, 42}

$$v_2 \approx \frac{1}{2} \frac{R_{AA}^{in} - R_{AA}^{out}}{R_{AA}^{in} + R_{AA}^{out}}. \quad (4)$$

It is worth noting that experimental approach to v_2 is different from Eq. (4). However, to our knowledge, and as already discussed in Ref. 21, that approach could lead to different elliptic flow predictions if event-by-event fluctuations are taken into account, which is out of the scope of this study.

3. Reliability of the Framework

The reliability of DREENA-B framework, outlined in the previous section, is tested against experimentally available data at the LHC in Ref. 17. Note that in generating all predictions we used no fitting parameters, *i.e.*, the parameters take their standard literature values. We obtained a very good agreement between our predictions and the existing data for: *i*) Both high- p_\perp R_{AA} and v_2 , so that long-standing v_2 puzzle⁴³ (inability of various models to jointly explain high- p_\perp R_{AA} and v_2 data, with tendency to underestimate v_2 compared to the experimental data) is naturally solved within our framework; *ii*) Diverse colliding systems, such as Pb + Pb at $\sqrt{s_{NN}} = 2.76$ TeV and 5.02 TeV, and Xe + Xe at $\sqrt{s_{NN}} = 5.44$ TeV; *iii*) Both light and heavy flavor particles, that is, h^\pm , D , B mesons, and *iv*) All available centrality ranges.

4. Results and Discussion

In this section, first, we define the four commonly considered temperature profiles,¹⁴ which differ only at early times. Next, we assess their effects on our full-fledged

predictions for high- p_\perp angular averaged and angular differential nuclear modification factors. Finally, we revise the soundness of the commonly applied multiple fitting procedure. For each result, we provide an intuitive explanation based on R_{AA} asymptotic scaling behavior. For more details, we refer the reader to Ref. 21.

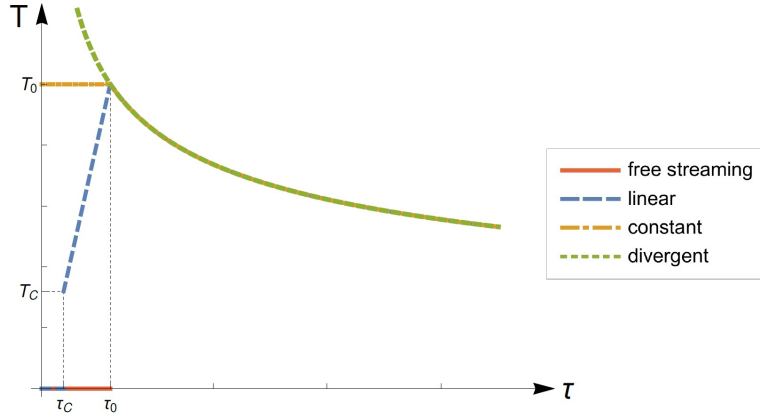


Fig. 1. Four simplified temperature profiles, with the same 1D Bjorken¹⁸ temperature evolution after thermalization ($\tau \geq \tau_0$), and whose differences before thermalization mimics different evolutions at initial stage ($\tau < \tau_0$). These diverse initial-stage cases are: the *free-streaming* (full red curve), the *linear* (dashed blue curve), the *constant* (dot-dashed orange curve) and *divergent* case (dotted green curve), as denoted in the legend. Figure adapted from Ref. 21.

4.1. Effect of different initial stages on high- p_\perp R_{AA} and v_2

Now that framework is set and tested, for the study covered by this paper, next we concentrate on four commonly assumed temperature profiles¹⁴ that consider the same 1D Bjorken¹⁸ temperature profile after, but differ before the thermalization ($\tau < \tau_0$). More particularly, in Fig. 1, we distinguish:

- the *free-streaming* case (full red curve), which corresponds to omitting the energy loss before the QGP thermalization;
- the *linear* case (dashed blue curve), which corresponds to linearly increasing T with proper time from transition temperature ($T_C = 160$ MeV,⁴⁰ $\tau_C = 0.25$ fm) to the initial temperature T_0 of equilibrated plasma, otherwise $T = 0$;
- the *constant* case (dot-dashed orange curve), with T equal to the initial temperature T_0 ; and
- the *divergent* case (dotted green curve), corresponding to 1D Bjorken evolution from the beginning $\tau = 0$.

First, we assess to what extent high- p_\perp R_{AA} is affected by the presumed initial stages depicted in Fig. 1. From the left column of Fig. 2, we infer that high- p_\perp

R_{AA} is sensitive to the initial stages. Particularly, we see that for both light and heavy flavor particles, suppression is the lowest in the *free-streaming* case, while progressively increasing toward the *divergent* case, which is expected due to an increase in energy loss. Unfortunately, the discrepancies between these curves are not very distinguishing, and within the current error bars, one is unable to differentiate between these different scenarios.

Next, we investigate the sensitivity of high- p_\perp elliptic flow to the initial stages. Unexpectedly, from the right column of Fig. 2, we observe that v_2 is insensitive to the presumed initial stages for all types of particles, contrary to the conclusion derived in Ref. 16. Therefore, from our study, it follows that v_2 cannot differentiate between different initial-stage scenarios.

To quantitatively explain the obtained results, we plot heavy flavor momentum dependence of proportionality functions, which are defined in the following manner:

$$\gamma_i^{in} = \frac{R_{AA,i}^{in}}{R_{AA,fs}^{in}}, \quad \gamma_i^{out} = \frac{R_{AA,i}^{out}}{R_{AA,fs}^{out}}, \quad \gamma_i = \frac{R_{AA,i}}{R_{AA,fs}}, \quad (5)$$

where $i \in \{lin, const, div\}$. The results and conclusions for charged hadrons are the same and are shown in Ref. 21. Thus, in Fig. 3, we distinguish three sets of curves (corresponding to *linear*, *divergent*, and *constant* cases relative to *free-streaming* case), each of which contains corresponding three proportionality functions. The most important observation from Fig. 3 is that within the same set of curves the proportionality functions are practically identical for the relations involving R_{AA}^{in} , R_{AA}^{out} and R_{AA} , that is

$$\gamma_i^{in} \approx \gamma_i^{out} \approx \gamma_i. \quad (6)$$

It is worth noting that $\gamma_i < 1$, and that for $i \neq j \rightarrow \gamma_i(p_\perp) \neq \gamma_j(p_\perp)$. If we recall that high- p_\perp R_{AA} and v_2 are given by Eqs. (3) and (4), it is straightforward to show that only R_{AA} , and not v_2 is affected. More specifically, for any i we obtain:

$$R_{AA,i} \approx \frac{\gamma_i(R_{AA,fs}^{in} + R_{AA,fs}^{out})}{2} = \gamma_i R_{AA,fs}, \quad (7)$$

$$v_{2,i} \approx \frac{1}{2} \frac{\gamma_i(R_{AA,fs}^{in} - R_{AA,fs}^{out})}{\gamma_i(R_{AA,fs}^{in} + R_{AA,fs}^{out})} = v_{2,fs}, \quad (8)$$

as observed in Fig. 2.

As an additional test of v_2 equivalence for different initial stages, in Fig. 4, we present the ratio of elliptic flow in *linear*, *constant* and *divergent* cases relative to the *free-streaming* case. From Fig. 4, which is a counterpart of Fig. 3, we observe that these ratios are consistent with unity for both D and B mesons. The result is the same for charged particles and omitted for consistency. Note that our predictions are valid for $p_\perp \gtrsim 10$ GeV. This, furthermore, confirms the conclusions obtained

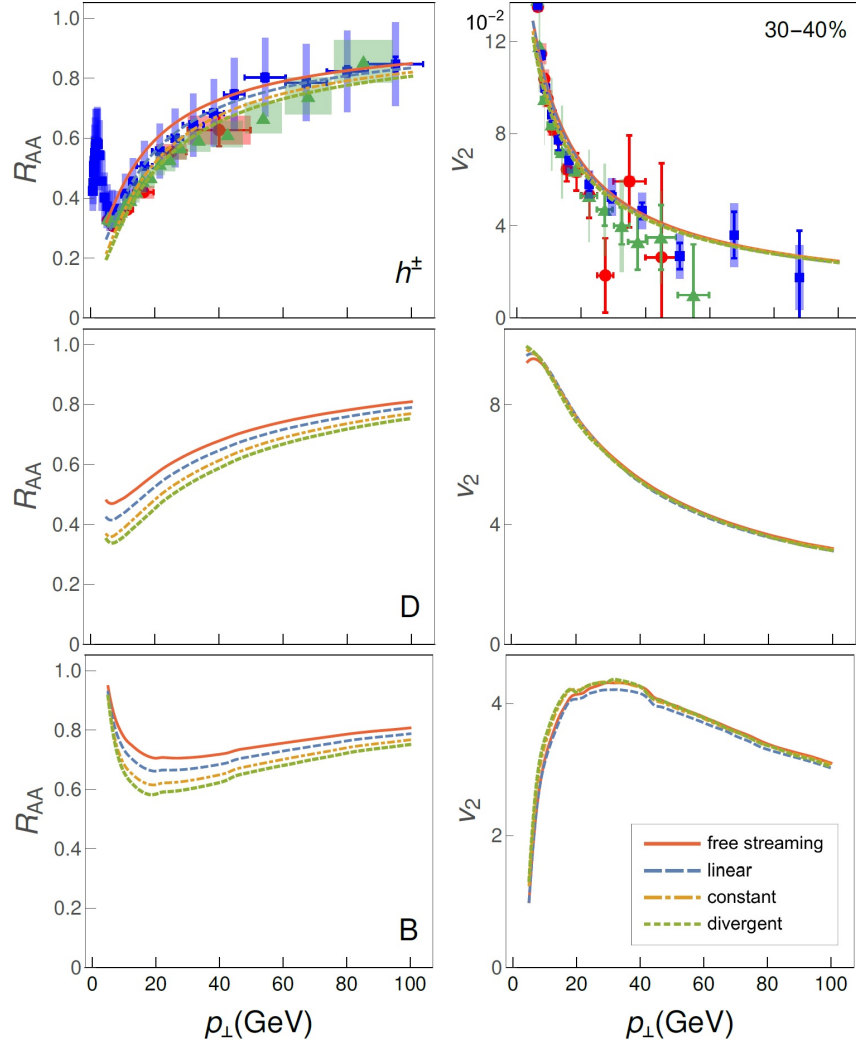
Utilizing high- p_{\perp} theory and data to constrain the initial stages of QGP 7

Fig. 2. Sensitivity of high- p_{\perp} observables to different initial stages presented in Fig. 1. The left (right) column corresponds to high- p_{\perp} R_{AA} (v_2) vs p_{\perp} . Charged hadron, D meson and B meson predictions are presented in upper, middle and lower row, respectively. Charged hadron R_{AA} predictions are compared with 5.02 TeV Pb + Pb CMS⁸ (blue squares), ATLAS⁹ (green triangles) and ALICE¹⁰ (red circles) h^{\pm} R_{AA} data in the upper left plot, while its v_2 predictions are compared with the corresponding 5.02 TeV Pb + Pb CMS¹¹ (blue squares), ATLAS¹² (green triangles) and ALICE¹³ (red circles) h^{\pm} data in the upper right plot. In each plot, full red curve corresponds to the *free-streaming* case, dashed blue curve to the *linear* case, dot-dashed orange curve to the *constant* case, and dotted green curve to the *divergent* case, as indicated in legend. The results are presented for the centrality range 30 – 40%, and $\mu_M/\mu_E = 0.5$. Figure adapted from Ref. 21.

from Fig. 2 (right column) and Fig. 3, as well as the validity of our quantitative analysis (given by Eqs. (7) and (8)).

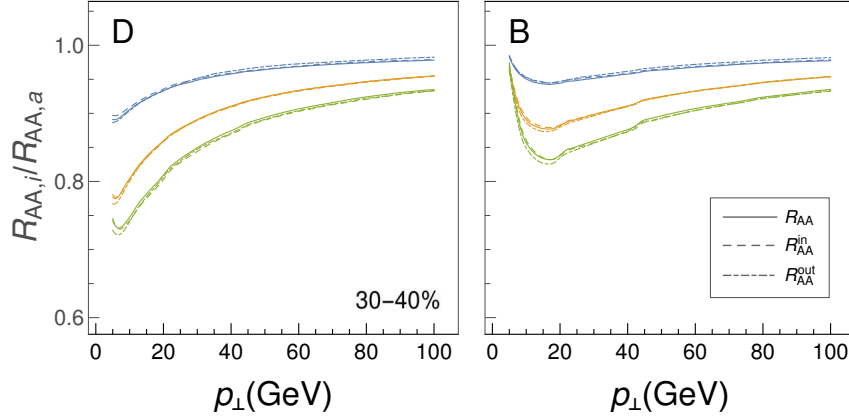


Fig. 3. R_{AA}^{in} (dashed curves), R_{AA}^{out} (dot-dashed curves) and R_{AA} (full curves) vs p_{\perp} in *linear* (blue set of curves), *constant* (orange set of curves) and *divergent* case (green set of curves) relative to the *free-streaming* case. The left (right) plot corresponds to D (B) mesons. The parameters are the same as in Fig. 2.

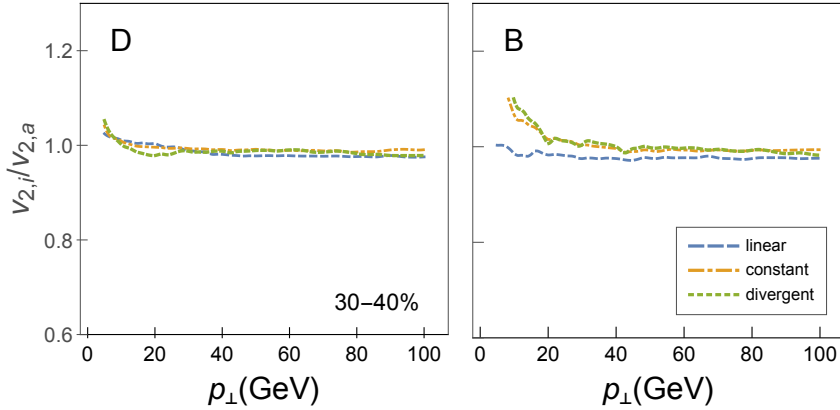


Fig. 4. v_2 in *linear* (dashed blue curves), *constant* (dot-dashed orange curves) and *divergent* case (dotted green curves) vs p_{\perp} relative to the *free-streaming* case. The left (right) plot corresponds to D (B) mesons. The parameters are the same as in Fig. 2.

Additionally, R_{AA} sensitivity to the initial stages is in a qualitative agreement with Refs. 17, 44, 45, where it was shown that high- p_{\perp} R_{AA} is only sensitive to the averaged properties of the evolving medium, such as average T (\bar{T}), *i.e.*, the analytical estimate reads:

$$R_{AA} \sim \frac{\Delta E}{E} \sim \bar{T}. \quad (9)$$

The fact that \bar{T} s are different for all four initial-stage cases (see Fig. 1) results in observed R_{AA} differences.

4.2. Revision of commonly used multiple fitting procedure

Finally, in this subsection, we test an approach commonly used in Refs. 16,41,46–49, in which the energy loss is fitted for the initial-stage cases (see Fig. 1), via the change of multiplicative fitting factor in the energy loss to reproduce the high- p_\perp R_{AA} experimental data. More specifically, in our full-fledged calculations we introduce an additional multiplicative fitting factor C_i^{fit} , which is estimated for each initial-state case as the best fit to the *free-streaming* R_{AA} , since free-streaming is commonly considered scenario in both low- and high- p_\perp sector^a. We observe²¹ a decreasing trend in multiplicative fitting factors from the *free streaming* toward the *divergent* case, as expected, to annul the higher energy losses in corresponding cases compared to the *free-streaming* one.

Thus obtained (fitted) R_{AA} s are presented in the left plot of Fig. 4, and are practically overlapping, as expected. However, the right plot of Fig. 4 shows that through this fitting procedure high- p_\perp v_2 is significantly affected, that is, the highest value is in the *free-streaming* case, while the lowest is in the *divergent* case. This observation could evoke a naive interpretation that initial stages, that is, the only region in which T profiles differ, are responsible for these discrepancies. However, that would be inconsistent with our results presented in the previous subsection, as well as with intuitive anticipation that the introduction of the energy loss at the initial stage should affect R_{AA} .

To provide a quantitative explanation of the obtained results in Fig. 4, we apply asymptotic scaling behavior of R_{AA} ,^{17,26} which mimics our complex suppression procedure for very high- p_\perp jets and at higher centralities:

$$R_{AA} = 1 - \xi \bar{T}^m \bar{L}^n, \quad (10)$$

where \bar{L} denotes the average path length traversed by the jet. The corresponding \bar{T} and \bar{L} proportionality factors – $m \approx 1.2$ and $n \approx 1.4$ are estimated in Refs. 50 and 51, respectively. ξ stands for a proportionality factor, which depends on jet's p_\perp and flavor.

By introducing multiplicative fitting factor in energy loss (see Eq. (9)), and making use of Eq. (10), the fitted R_{AA} s in high- p_\perp limit now read:

$$R_{AA,i}^{fit} \approx 1 - C_i \xi \bar{T}_i^m \bar{L}_i^n \approx 1 - C_i (1 - R_{AA,i}), \quad (11)$$

where $i = lin, const, div$ and C_i s are high- p_\perp limits of corresponding C_i^{fit} s. Note that Eqs. (10) and (11) (in their original form) are applicable to R_{AA}^{in} and R_{AA}^{out} as

^aThe estimated²¹ values of C_i^{fit} are: 1, 0.87, 0.74 and 0.67 in *free streaming*, *linear*, *constant* and *divergent* cases, respectively.

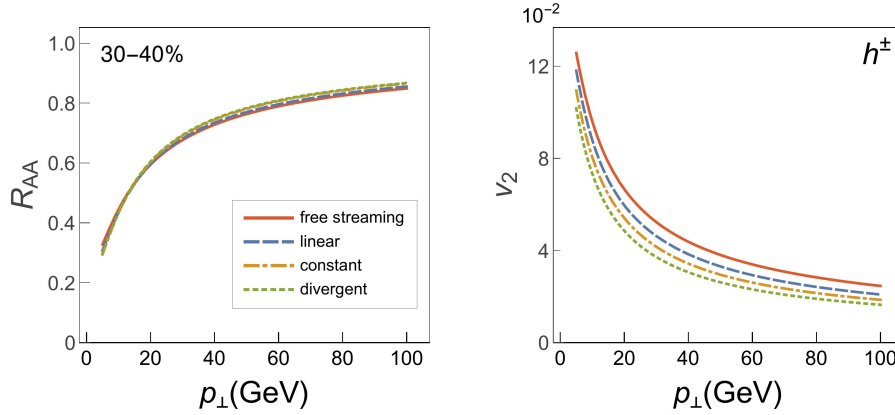


Fig. 5. Sensitivity of charged hadron high- p_{\perp} R_{AA} (left plot) and v_2 (right plot) to different initial-stage cases from Fig. 1, when a multiplicative factor is included in energy loss to reproduce the *free-streaming* R_{AA} . In each plot, full red curve corresponds to the *free-streaming* case, dashed blue curve to the *fitted linear* case, dot-dashed orange curve to the *fitted constant* case, and dotted green curve to the *fitted divergent* case, as indicated in legend. The parameters are the same as in Fig. 2. Figure adapted from Ref. 21.

well (the same multiplicative fitting factor is naturally applied in all three cases). In order for $R_{AA,i}^{fit}$ to reproduce the free streaming R_{AA} , *i.e.*,

$$R_{AA,i}^{fit} = R_{AA,fs}, \quad (12)$$

it is straightforward to obtain:

$$\begin{aligned} v_{2,i}^{fit} &\approx \frac{1}{2} \frac{C_i(R_{AA,i}^{in} - R_{AA,i}^{out})}{2R_{AA,fs}} = \frac{1}{2} \frac{C_i \gamma_i (R_{AA,fs}^{in} - R_{AA,fs}^{out})}{R_{AA,fs}^{in} + R_{AA,fs}^{out}} \\ &= C_i \gamma_i v_{2,fs}, \end{aligned} \quad (13)$$

where along with Eq. (12), we applied Eqs. (3)-(6), and Eqs. (10), (11), together with their out- and in-plane counterparts.

From Eq. (13) it follows that the reasons behind v_2 decrease in *linear*, *constant* and *divergent* cases compared to the *free streaming* one are the multiplicative fitting factor C_i and proportionality function γ_i , both of which are smaller than 1. However, note that γ_i approaches to 1 at high p_{\perp} (we refer the reader to Fig. 3), so that the diminishing of v_2 compared to the *free streaming* case is predominantly a consequence of a decrease in the imposed fitting factor and not the initial stages as obtained in Ref. 16. We thus infer that the common procedure in which the energy loss fitting factor is repeatedly adjusted for each initial stage may lead to misconceptions about the underlying physical mechanisms.

5. Conclusions and Outlook

We here addressed whether, and to what extent, we can use high- p_{\perp} observables to explore the initial stages before QGP thermalization. To this end, we studied how four different commonly considered initial stage scenarios, which have the same temperature profile after, but differ in the temperature profiles before thermalization, affect high- p_{\perp} R_{AA} and v_2 predictions, stemming from our DREENA-B¹⁷ framework combined with 1D Bjorken expansion.¹⁸ We surprisingly obtained that high- p_{\perp} v_2 is insensitive to the presumed initial stages, as opposed to high- p_{\perp} R_{AA} . However, within the current error bars, R_{AA} sensitivity does not allow differentiation between different initial stage cases. Moreover, we inferred that the previously reported sensitivity of high- p_{\perp} v_2 to initial stages is mostly an artifact of the fitting procedure. Consequently, a common procedure, where free parameters in energy loss are separately fitted for each initial stage may obscure the understanding of the underlying physical mechanisms. In general, our results imply that the simultaneous study of high- p_{\perp} R_{AA} and v_2 , with restrained temperature profiles (isolating the differences in the initial states) and unchanged energy loss parametrization throughout the study, is needed to set reliable constraints on the initial stages in the future.

Acknowledgements

This work is supported by the European Research Council, grant ERC-2016-COG: 725741, and by the Ministry of Science and Technological Development of the Republic of Serbia, under project No. ON171004 and No. ON173052.

References

1. J. C. Collins and M. J. Perry, *Phys. Rev. Lett.* **34** 1353 (1975).
2. S.S. Adler *et al.*, [PHENIX Collaboration], *Phys. Rev. Lett.* **91** (2003) 072303.
3. M. Gyulassy and L. McLerran, *Nucl. Phys. A* **750** (2005) 30.
4. B. Jacak and P. Steinberg, *Phys. Today* **63** (2010) 39.
5. F. Gelis and B. Schenke, *Ann. Rev. Nucl. Part. Sci.* **66** (2016) 73.
6. G. Aad *et al.* [ATLAS Collaboration], *JHEP* **1311** (2013) 183.
7. H. Niemi, G. S. Denicol, H. Holopainen and P. Huovinen, *Phys. Rev. C* **87** (2013) 054901.
8. V. Khachatryan *et al.* [CMS Collaboration], *JHEP* **1704** (2017) 039.
9. The ATLAS collaboration [ATLAS Collaboration], ATLAS-CONF-2017-012.
10. S. Acharya *et al.* [ALICE Collaboration], *JHEP* **1811**, 013 (2018).
11. A. M. Sirunyan *et al.* [CMS Collaboration], *Phys. Lett. B* **776** (2018) 195.
12. M. Aaboud *et al.* [ATLAS Collaboration], *Eur. Phys. J. C* **78** (2018) 997.
13. S. Acharya *et al.* [ALICE Collaboration], *JHEP* **1807** (2018) 103.
14. J. Xu, A. Buzzatti and M. Gyulassy, *JHEP* **1408** (2014) 063.
15. R. Katz, C. A. G. Prado, J. Noronha-Hostler, J. Noronha and A. A. P. Suaide, *Phys. Rev. C* **102** (2020) 024906.
16. C. Andres, N. Armesto, H. Niemi, R. Paatelainen and C. A. Salgado, *Phys. Lett. B* **803** (2020) 135318.

12 *Bojana Ilic, Dusan Zigic, Marko Djordjevic, Magdalena Djordjevic*

17. D. Zigic, I. Salom, M. Djordjevic and M. Djordjevic, *Phys. Lett. B* **791** (2019) 236.
18. J. D. Bjorken, *Phys. Rev. D* **27** (1987) 140.
19. M. Djordjevic and M. Djordjevic, *Phys. Lett. B* **734** (2014) 286.
20. E. Molnar, H. Holopainen, P. Huovinen and H. Niemi, *Phys. Rev. C* **90** (2014) 044904.
21. D. Zigic, B. Ilic, M. Djordjevic and M. Djordjevic, *Phys. Rev. C* **101** (2020) 064909.
22. S. Wicks, W. Horowitz, M. Djordjevic and M. Gyulassy, *Nucl. Phys. A* **784** (2007) 426.
23. Z. B. Kang, I. Vitev and H. Xing, *Phys. Lett. B* **718** (2012) 482; R. Sharma, I. Vitev and B.W. Zhang, *Phys. Rev. C* **80** (2009) 054902.
24. M. Gyulassy, P. Levai and I. Vitev, *Phys. Lett. B* **538** (2002) 282.
25. A. Dainese, *Eur. Phys. J. C* **33** (2004) 495.
26. D. Zigic, I. Salom, J. Auvinen, M. Djordjevic and M. Djordjevic, *J. Phys. G* **46** (2019) 085101.
27. D. de Florian, R. Sassot and M. Stratmann, *Phys. Rev. D* **75** (2007) 114010.
28. M. Cacciari, P. Nason, *JHEP* **0309** (2003) 006; E. Braaten, K.-M. Cheung, S. Fleming and T. C. Yuan, *Phys. Rev. D* **51** (1995) 4819.
29. V. G. Kartvelishvili, A.K. Likhoded, V.A. Petrov, *Phys. Lett. B* **78** (1978) 615.
30. M. Djordjevic, *Phys. Rev. C* **80** (2009) 064909.
31. M. Djordjevic and U. Heinz, *Phys. Rev. Lett.* **101** (2008) 022302.
32. M. Djordjevic, *Phys. Rev. C* **74** (2006) 064907.
33. J. I. Kapusta, *Finite-Temperature Field Theory* (Cambridge University Press, Cambridge, 1989).
34. M. Djordjevic, *Phys. Lett. B* **709** (2012) 229.
35. Yu. Maezawa *et al.* [WHOT-QCD Collaboration], *Phys. Rev. D* **81** (2010) 091501.
36. A. Nakamura, T. Saito and S. Sakai, *Phys. Rev. D* **69** (2004) 014506.
37. B. Blagojevic, M. Djordjevic and M. Djordjevic, *Phys. Rev. C* **99** (2019) 024901.
38. B. Blagojevic and M. Djordjevic, *J. Phys. G* **42** (2015) 075105.
39. J. E. Bernhard, J. S. Moreland and S. A. Bass, *Nucl. Phys. A* **967** (2017) 293.
40. A. Bazavov *et al.* [HotQCD Collaboration], *Phys. Rev. D* **90** (2014) 094503.
41. B. Betz and M. Gyulassy, *JHEP* **1408** (2014) 090 [Erratum: *JHEP* **1410** (2014) 043].
42. P. Christiansen, K. Tywoniuk and V. Vislavicius, *Phys. Rev. C* **89** (2014) 034912.
43. S. K. Das, F. Scardina, S. Plumari and V. Greco, *Phys. Lett. B* **747** (2015) 260.
44. T. Renk, *Phys. Rev. C* **85** (2012) 044903.
45. D. Molnar and D. Sun, *Nucl. Phys. A* **932** (2014) 140; **910-911** (2013) 486.
46. J. Noronha-Hostler, B. Betz, J. Noronha and M. Gyulassy, *Phys. Rev. Lett.* **116** (2016) 252301.
47. B. Betz, M. Gyulassy, M. Luzum, J. Noronha, J. Noronha-Hostler, I. Portillo and C. Ratti, *Phys. Rev. C* **95** (2017) 044901.
48. C. A. G. Prado, J. Noronha-Hostler, R. Katz, A. A. P. Suaide, J. Noronha, M. G. Munhoz and M. R. Cosentino, *Phys. Rev. C* **96** (2017) 064903.
49. S. Cao *et al.* [JETSCAPE Collaboration], *Phys. Rev. C* **96** (2017) 024909.
50. S. Stojku, B. Ilic, M. Djordjevic, M. Djordjevic, *Phys. Rev. C* **103** (2021) 024908.
51. M. Djordjevic, D. Zigic, M. Djordjevic, J. Auvinen, *Phys. Rev. C* **99** (2019) 061902.